UCRL-17249

University of California

Ernest O. Lawrence Radiation Laboratory

DEFECTS IN NEUTRON IRRADIATED MOLYBDENUM

TWO-WEEK LOAN COPY

This is a Library Circulating Copy which may be borrowed for two weeks. For a personal retention copy, call Tech. Info. Division, Ext. 5545

DISCLAIMER

This document was prepared as an account of work sponsored by the United States Government. While this document is believed to contain correct information, neither the United States Government nor any agency thereof, nor the Regents of the University of California, nor any of their employees, makes any warranty, express or implied, or assumes any legal responsibility for the accuracy, completeness, or usefulness of any information, apparatus, product, or process disclosed, or represents that its use would not infringe privately owned rights. Reference herein to any specific commercial product, process, or service by its trade name, trademark, manufacturer, or otherwise, does not necessarily constitute or imply its endorsement, recommendation, or favoring by the United States Government or any agency thereof, or the Regents of the University of California. The views and opinions of authors expressed herein do not necessarily state or reflect those of the United States Government or any agency thereof or the Regents of the University of California.

Submitted to Acta Metallurgica

UCRL-17249
Preprint

UNIVERSITY OF CALIFORNIA

Lawrence Radiation Laboratory
Berkeley, California

AEC Contract No. 2-7405-eng-48

DEFECTS IN NEUTRON IRRADIATED MOLYBDENUM

P. Rao and G. Thomas

November 1966

DEFECTS IN NEUTRON IRRADIATED MOLYBDENUM

P. Rao and G. Thomas

Inorganic Materials Research Division, Lawrence Radiation Laboratory
and Department of Mineral Technology, College of Engineering,
University of California, Berkeley, California

ABSTRACT

Molybdenum of purity 99.965% has been examined by transmission electron microscopy and field ion microscopy before and after neutron irradiation to 1×10^{19} nvt at reactor ambient temperature. The structure after 1 hour anneal at 760°C following irradiation was also investigated. Dark field strain contrast analysis has shown that the defects induced by irradiation are in the form of small (~100Å dia, grown to ~ 200Å dia after the anneal) perfect prismatic dislocation loops of the {110} a/2 <111> type. The loops are identified, within the limits of strain contrast theory, to be mostly interstitial in character. Field ion micrographs taken of specimens made from foils previously examined by electron microscopy, failed to reveal any vacancies, although images characteristic of interstitials and/or interstitial impurity atoms were obtained. The results are discussed in terms of the known irradiation behavior of molybdenum.

I. INTRODUCTION

Previous work, using transmission electron microscopy[1-5] and field ion microscopy,[6] on neutron irradiated BCC metals, has shown that the damage is introduced in the form of point defects (observable as single defects by field ion microscopy) which cluster to produce prismatic dislocation loops (observable by electron microscopy).

Downey and Eyre[1] observed point defect clusters in molybdenum irradiated at reactor ambient temperatures. The defects were deduced to be interstitial in character. Little change in substructure was observed on annealing up to 800°C, while the microhardness showed a peak at 170°C followed by a steady recovery. Above 800°C, the loops were observed to grow rapidly and finally joined up to form dislocation networks, and there was a corresponding increase in the rate of recovery of microhardness. Meakin and Greenfield[2] produced a low density of resolvable loops directly during irradiation by subjecting molybdenum to neutron irradiation at 600°C. Mastel and Brimhall[3] suggested that carbon in molybdenum neutron irradiated at 40°C promotes the heterogeneous nucleation of clusters and is responsible for the formation of resolvable dislocation loops. In all the work reported to date, the loops have been deduced to be interstitial in nature, with Burgers vector a/2 <111> and loop plane {110}. A few dislocation loops with Burgers vector a<100> have also been observed at low annealing temperatures.[1] Very recently, Eyre and Downey[4] have shown that the nature of damage observed is dependent on the impurity content of molybdenum.

On the basis of the observations outlined above, Eyre and Bullough[5] predicted the formation of prismatic loops in irradiated BCC metals, with {110} loop planes and $\vec{b}$ = a/2<111>or $\vec{b}$ = a<100>. Taking elastic energy

considerations into account, Eyre and Bullough concluded that both the a/2<111> and a<100> loops lie on {110} and are initially rectilinear but should grow into circular loops and rotate into the pure edge orientation, similar to the behavior of perfect loops in FCC metals. Analysis of non-edge prismatic dislocation loops is possible from the geometry of the double-arc diffraction contrast, if the loops are large enough.[7,8]

However, for dislocation loops smaller than about 200Å, the images of their sides are not clearly resolvable (as in the case of "black spot" defects observed in the bright field images of irradiated foils). Diffraction contrast then becomes unsuitable for analyzing small defects and, therefore, strain contrast imaging must be used in identifying dislocation loops, as has been shown for irradiated or quenched copper,[9,10,11] and other small defects in FCC crystals.[12-14]

The analysis of the loop plane and Burgers vector of strain contrast images from prismatic loops in FCC and BCC metals have been considered elsewhere.[7-9] The validity of the strain contrast theory and its applicability to the determination of defect character have been considered in great detail by Bell et. al.[13] It has been shown that the foil thickness, the extinction distance, the deviation parameter, the anomalous absorption parameter, the defect size, defect shape, defect position in the foil, inclination of the defect with respect to the incident beam, defect density and the operating reflection are the parameters which have to be considered for both the bright and dark field cases.[13] In order to determine the character of defects, it is essential to know the exact position in the foil, since the analysis of Ashby-Brown[14] is only applicable to defects within half an extinction distance of the surfaces.

Since imaging has not been previously employed specifically to investigate the nature of the small defects (so called black-spots), in neutron irradiated BCC metals, this investigation is partly devoted to this topic. The neutron dosage level and temperature of irradiation have been so chosen to give defect clusters small enough to be analyzed by strain contrast. Two specific cases have been selected. Irradiated molybdenum samples in the as-irradiated and irradiated-annealed conditions have been examined.

Previous work, using field-ion microscopy, on damage introduced by alpha particles,[15,16] helium ions,[17] fission fragments,[18] and neutrons[6] has led to the formulation of the nature of radiation induced defects of a few atomic dimensions. Single vacancies, divacancies and vacancy clusters have been most easily and unambiguously identified as missing atoms, although those inside the unresolved close-packed planes escape observation.[19] In order to be sure that the missing atom has not just been removed by field evaporation, only unoccupied sites in the interior of a fully resolved plane, or in the inner part of a homogeneous atom chain should be identified as vacancies. Interstitials have been identified as bright dots appearing at the surface showing up as a result of lattice relaxation.[20] The exact mechanism of image formation for these bright spots is not yet clear. Bright spots of a few atoms diameters have been observed to alternate with regions of relative perfection in neutron irradiated platinum. Impurities present would be expected to appear in a distinct way due to electronic and geometric mismatch at the surface.[19] Impurity atoms would stand out with higher brightness and fuzziness and could be confused with interstitials created by radiation damage.

In all the reported work to date, wire specimens have either been subjected to particle irradiation outside the field ion microscope or in situ. In the present work the microscope has been used for the first time to observe damage produced in bulk specimens subjected to neutron irradiation. A correlation between results obtained from transmission electron microscopy and field ion microscopy has been attempted.

II. EXPERIMENTAL PROCEDURE

A. Material and Irradiation

The specimens used in this investigation were obtained from arc vacuum cast recrystallized molybdenum sheet in the form of 20 mil thick strips. The analysis of the as-received molybdenum sheet is given in Table 1.* The post-test analysis is compared with the as-received analysis in Table 2.*

Table 1

Element	Fe	Si	Al	Ca	Cu	W	Sn	B	Ti	Zr	Ni	Cr	Mn
Parts per Million	21	20	5	4	2	100	10	10	1	1	1	1	1

Table 2

Element	As-Received (ppm)	Post Test (ppm)
O_2	25	13
H_2	2	1
N_2	5	2
C	150	160

*Chemical analysis supplied by Nuclear Materials and Propulsion Operation, General Electric Company, Cincinatti, Ohio.

Prior to irradiation the specimens were annealed in argon for one hour at 1200°C. Specimens were irradiated in an aluminum can stacked (by twos) between aluminum filler pieces, for heat removal, in a helium atmosphere. The irradiations were conducted in the Oak Ridge (ORN-23) reactor at a dosage level of ~1×10^{19} nvt, $E_n \geq 1$ Mev at reactor ambient temperature.** Some material was subsequently annealed at 760°C for one hour.

A new method for obtaining specimens for both electron and field ion microscopy from the same strip molybdenum was attempted, involving the thin foil technique for electron microscopy and preparation of sharp tips for field ion microscopy from bulk metal rather than from wires.

B. Specimen Preparation for Electron Microscopy

Electron transparent foils were obtained by electropolishing the 20 mil thick molybdenum strip by the window method in an electrolyte of 87.5% methyl alcohol and 12.5% sulfuric acid at 0°C using a D.C. voltage of 6-8 volts. In order to eliminate the possibility of interpreting polishing defects[21] or other artifacts on the surface[13] as defect clusters caused by irradiation, both the unirradiated control specimen and the as-irradiated specimen were electropolished together under identical conditions. The irradiated foils obtained had negligible ($\beta + \gamma$) activity.

A Siemens Elmiskop I microscope equipped with a double tilting stage was used in this investigation. The two-beam orientation necessary for contrast analysis of defects was readily obtained using the double tilting stage. Dark field images were formed by gun-tilting so as to obtain maximum resolution and contrast.[9] The foil orientations were

**Irradiation supervised by Nuclear Materials and Propulsion Operation, General Electric Company, Cincinatti, Ohio.

accurately determined from a composite BCC Kikuchi map described elsewhere,[22] and the usual rotations between image and diffraction pattern, have been taken into account.

C. Specimen Preparation for Field Ion Microscopy

A new technique was used for preparing specimens for field-ion microscopy from the bulk metal. The advantage of this method is the elimination of any discrepancies that might arise in carrying out a study of radiation damage using two different physical forms of the metal, namely strip and wire, thereby eliminating the differences in chemical composition between wire and strip entering the analysis of results. Conventional field-ion specimens are in the wire form.

Masked edges left over after electropolishing the 20 mil strip by the window method were used as the starting point for the field-ion specimens. The irregular wire-like pieces were electropolished using the thin layer electropolishing technique. The method involves dipping the specimen through a thin layer (5mm) of an aqueous solution of potassium cyanide (10%), floating on top of an inert liquid, carbon tetrachloride. An A.C. supply of 1-40 volts is used, with gas evolution always occurring during specimen preparation.

Great care was exercised in polishing in order to obtain as symmetrical a tip as possible. The specimens were made to revolve about their own axis whilst electropolishing in order to smooth out irregularities. Tip formation resulted easily and the field-ion images obtained were comparable to those observed from wire specimens.

III. EXPERIMENTAL RESULTS

A. General Observations

Initial examination of the molybdenum foil showed that most of the grains had a preferred orientation at and near {111} or {011}. Using the double tilting stage, {112}, {123}, {135} and {012} foil orientations could be obtained. This proved to be useful in that a large proportion of edge-on loops were obtained which facilitates the applicability of the strain contrast theory in dark field (i.e., $\bar{g} \cdot \bar{R}$ is maximum for contrast, where $\bar{R}$ is the displacement vector associated with the loop). Bright field micrographs of unirradiated molybdenum (Fig. 1a) were free of the defects which were observed in irradiated molybdenum. The bright field micrographs of as-irradiated (1×10^{19} nvt; $E_n \geq 1$MeV) molybdenum show a very large number of spot defects (Fig. 1b). Figure 1c shows the dark field micrograph of the same area as in Fig. 1b. The very large number of black-white lobed images makes analysis impossible. The high density of induced defects results in overlapping strain fields, and a number of reversals in contrast are evident on both sides of the extinction contours in the bright and dark field images. It can be assumed that these strain contrast images arise from radiation induced defects and not as a result of electropolishing,[21] since the unirradiated foil electropolished simultaneously did not show these defects. In addition, the number of observable defects increases towards the thicker regions of the foil, as would be expected of an evenly distributed damage structure. A count of the number of images observable in Fig. 1b shows that the defect density increases from 4×10^{16} defects per cm^3 at a foil thickness of $2t_o$, (where t_o is the extinction distance) to 6.4×10^{16} defects per cm^3 at a thickness

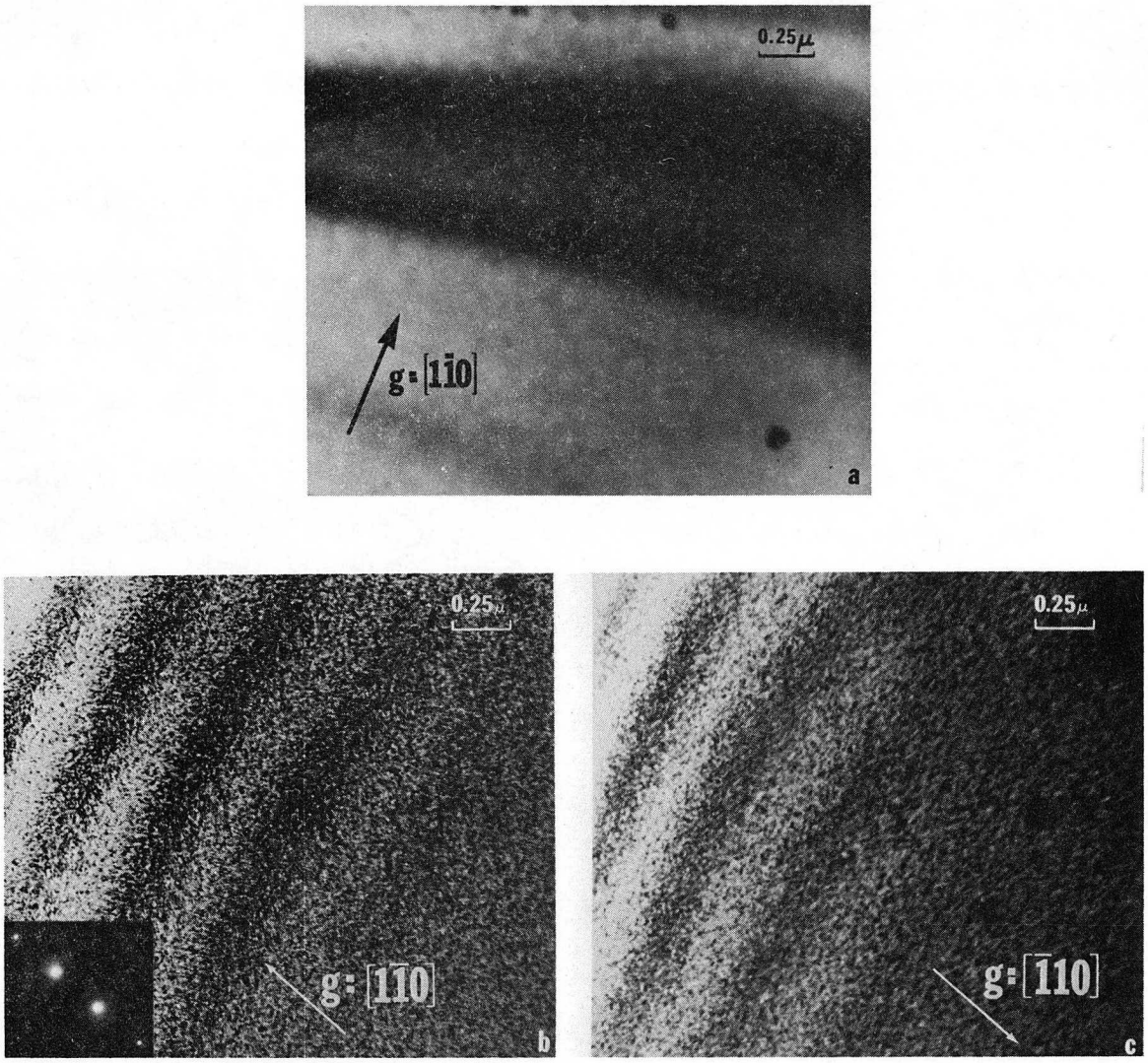

ZN-5929

Fig. 1 (a) Bright field micrograph of unirradiated molybdenum.
(b) Bright field micrograph of as-irradiated (1×10^{19} nvt; $E_n \geq 1$ MeV) molybdenum showing a very large number of spot defects. A defect density count shows that the number of observable defects increases with foil thickness.
(c) Dark field micrograph of the same irradiated area showing a high density of induced defects.

of $4t_o$. The strain contrast images are in best contrast at foil thickness of an odd number of one-quarter extinction distances.[9]

Experiments with irradiated molybdenum [$1x10^{19}$nvt; $E_n \geq$ 1MeV] annealed at 760°C for one hour yielded more interesting results. Three sets of experiments were performed. Firstly, the same area was observed in bright and dark field using different diffraction vectors, keeping s constant. Secondly, another area was observed in bright and dark field changing the sign of s while keeping the diffraction vector constant. In dark field for small values of $s \neq 0$, the defects are preferentially imaged near the top surface of the foil for $s < 0$ and at the bottom for $s > 0$.[23] Thirdly, an area was observed in dark field at $s < 0$ with different operative diffraction vectors.

B. Dependence of Strain-Contrast Images on the Diffraction Vector

The same specimen area can be imaged with different operating diffraction vectors, resulting in different extinction distances. Those dislocation loops which do not change sign for a sufficient variation of the extinction distance lie immediately below one of the surfaces, and statistically, therefore, the dark-field image would give the correct nature of these loops. That is, the number of "wrong sense" images decreases as the order of reflection increases.[10-13]

Figure 2 shows bright and dark field micrographs of the same area at $s > 0$. Figures 2a and 2b have the same <110> diffraction vector operating in bright and dark field, while Fig. 2c has a <112> diffraction vector operating on the same area in dark field..

The foil orientation, using both the <110> and <112> beams, was accurately determined using the BCC Kikuchi map developed by Okamoto

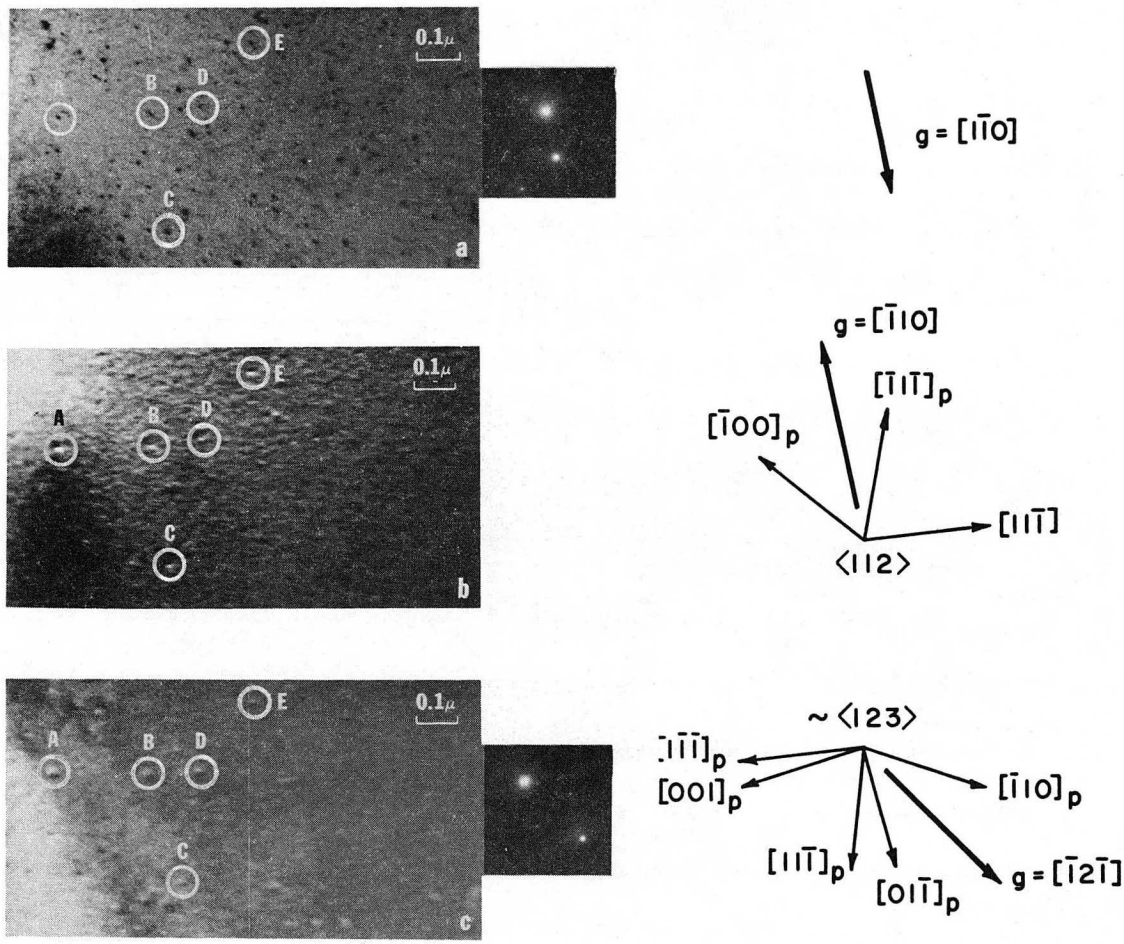

ZN-5926

Fig. 2. Bright and dark field micrographs of the same area in neutron irradiated (1×10^{19} nvt; $E_n \geq 1$ MeV) molybdenum annealed at 760°C for 1 hour. (a) and (b) have the same [1$\bar{1}$0] diffraction vector operating in bright and dark field, while (c) has a [$\bar{1}$2$\bar{1}$] diffraction vector operating in dark field. Comparison of the line of no contrast and streaking direction with the important ⟨100⟩, ⟨110⟩ and ⟨111⟩ projected directions shows that the defects A, B, C, D and E are of the same type - viz (01$\bar{1}$) loop planes and a/2[111] Burgers vectors.

et. al.[22] Stereograms suitably oriented give projections of the <111>, <110> and <011> directions which are of importance in BCC metals. As shown in Fig. 2, the lines of no contrast are distinctly normal to the projected <111> directions indicating that the Burgers vectors of these defects are of the type $\frac{a}{2}$<111>. The direction of black-white streaking is in the projected <110> directions, indicating that the loop planes of these planar defects are {110}.[7]

Examination of Figs. 2b and 2c show that all the black-white images (A,B,C,D and E) visible have the same (parallel) lines of no contrast and direction of streaking, and, therefore, have the same Burgers vector and loop plane. Since in (b) and (c) the lines of no contrast and the direction of black-white streaking do not change with the two different diffraction vectors, it is evident that the Burgers vector and loop plane of these defects are independent of the operating diffraction vector, and therefore, must be plate shaped defects, i.e., loops.[7]

C. Dependence of Strain Contrast Images on the Sign of s.

The sign of the deviation parameter s determines which part of the foil is in good contrast. In dark field, when $s < 0$, the top of the foil is in good contrast while when $s > 0$, the bottom of the foil is in good contrast.[13,23] Using these two imaging conditions, the position of the defect in the foil can be estimated positively for lower order beams. However, when $s \neq 0$, the effective extinction distance is decreased.

Figures 3 and 4 show areas of irradiated - annealed molybdenum observed in bright and dark field with the same operating <112> beam under conditions of s negative and s positive. The approximate position of each of the marked defects, determined on the basis of visibility under

different signs of s, are tabulated in Tables 3 (for Fig. 3) and 4 (for Fig. 4). An analysis of the Burgers vector and loop plane of each defect is also given.

Some of the larger defects show faint double-arc contrast in bright field. Loops unsuitably oriented to give good strain contrast images lie at small angles to the plane of the foil and will give good double arc contrast.[8,12] Defect X in Fig. 3, for example, shows double arc contrast with a clear line of no contrast parallel to the $[10\bar{1}]$ projected direction with the $[1\bar{1}1]$ projected direction normal to the line of no contrast. The displacement of the double-arc image is in the $[0\bar{1}0]$ projected direction. According to the double-arc model,[7,8] the loop plane of this particular loop is $[\bar{1}0\bar{1}]$ and Burgers vector $\frac{a}{2}\langle 1\bar{1}1\rangle$.

D. Determination of Defect Densities

An estimation of the density of defect clusters was attempted using bright field electron micrographs enlarged to a magnification of 200,000x. A count of the number of defects per unit volume in both the as-irradiated and irradiated-annealed states was made near the edge of the foil where extinction contours allow the foil thickness to be estimated. The diameter of the loops is measured along the line dividing the black-white lobed regions of the image. This dimension is relatively insensitive to the imaging conditions. The results are shown in Table 5.

The high density of defects in the as-irradiated foils makes it difficult to distinguish between superimposed clusters. The number of clusters/cm^3 can be compared to the theoretical number of displacements per unit volume. Using the Kinchin and Pease model,[24] and the values of each of these variables suggested for molybdenum by Downey and Eyre,[1]

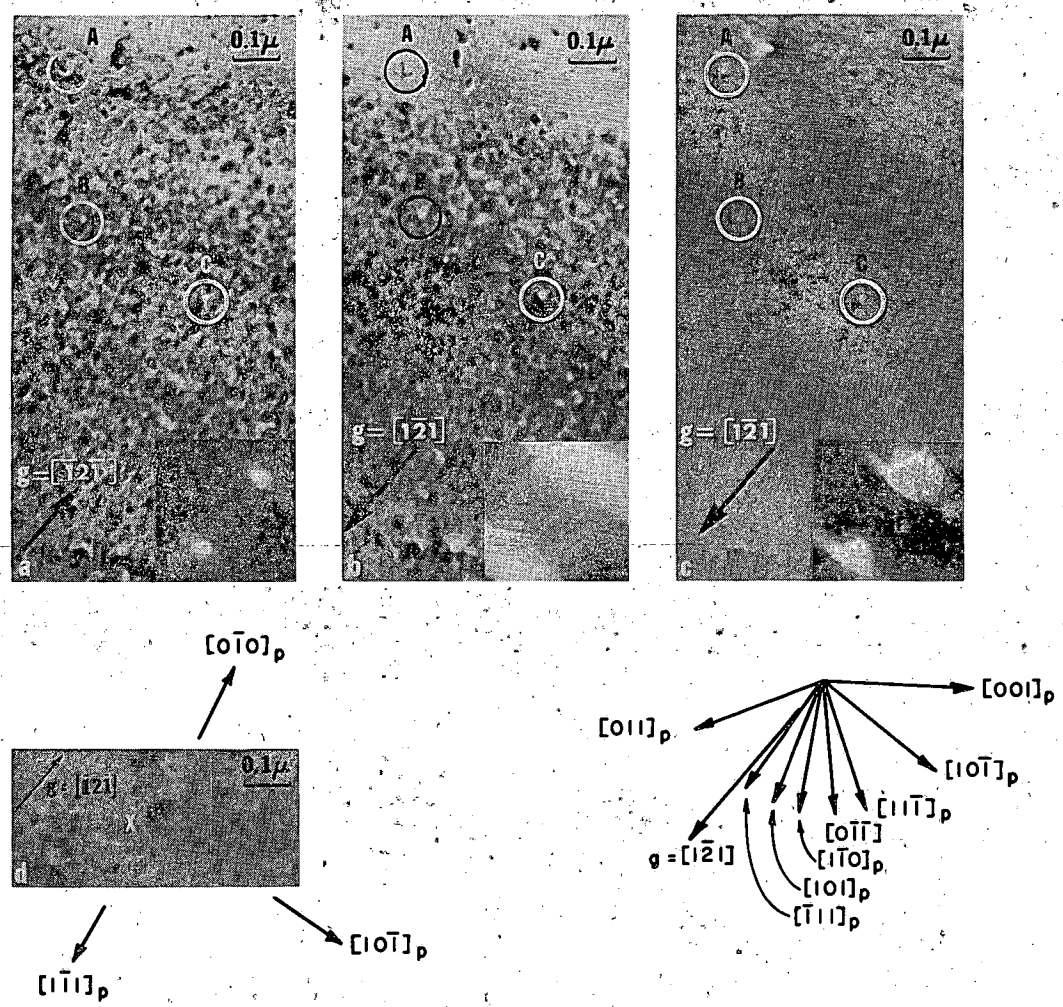

ZN-5927

Fig. 3. Bright and dark field images with the same operating [1$\bar{2}$1] beam. (a) Bright field micrograph, (b) dark field images at s < 0 bringing the top of the foil into good contrast; (c) dark field images at s > 0 bringing the bottom of the foil into good contrast; the approximate positions of each of the marked defects are tabulated alongside with an analysis of the Burgers vector and loop plane of each defect; (d) double arc contrast shown by a defect, X, is analyzed in terms of the line of no contrast being parallel to a projected ⟨110⟩ direction and normal to a projected ⟨111⟩ direction.

TABLE 3 (for Fig. 3)

Defect	Bright Field	Dark Field $s < 0$	Dark Field $s > 0$	Burgers Vector	Loop Plane	Approximate Position in Foil
A	Barely Visible	Invisible	Visible	<111>	{110}	Bottom
B	Barely Visible	Barely Visible	Visible	<111>	{110}	Bottom
C	Barely Visible	Clearly Visible	Visible	<111>	{110}	Top

Foil Orientation: Between [111] and [012] - 14° from [111]

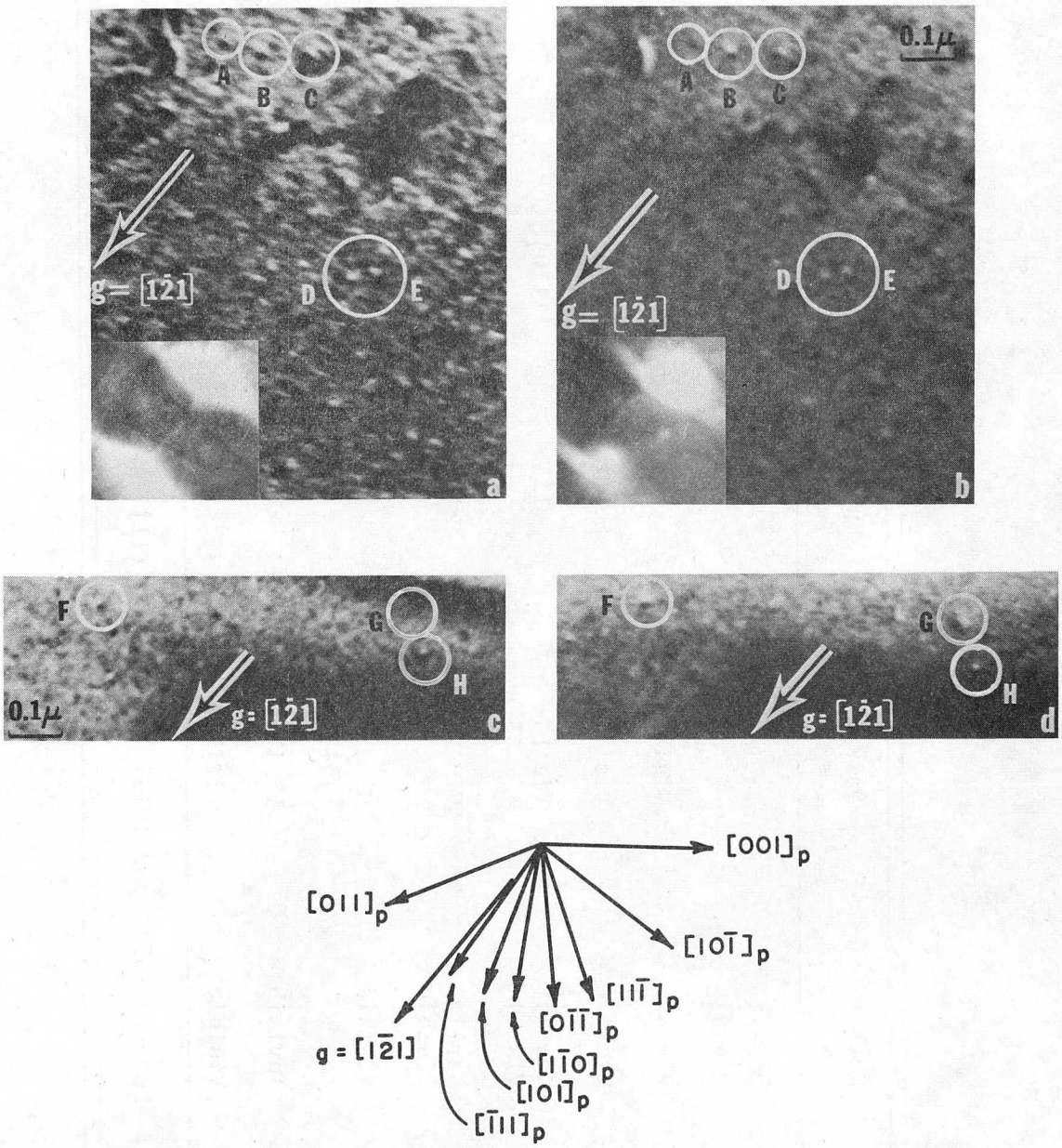

Fig. 4. Dark field images with the same operating [1$\bar{2}$1] beam. (a) and (c) are at s < 0 while (b) and (d) are at s > 0. The approximate positions of each of the marked defects along with their loop plane and Burgers vector analysis are tabulated alongside, as in Table 4.

TABLE 4 (for Fig. 4)

Defect	Dark Field $s < 0$	Dark Field $s > 0$	Burgers Vector	Loop Plane	Approximate Position in Foil
A	Clearly visible	Invisible	<111>	{110}	Top
B	Visible	Visible	<111>	{110}	Middle
C	Visible	Visible	<111>	{110}	Middle
D	Barely Visible	Visible	<111>	{110}	Bottom
E	Barely Visible	Visible	<111>	{110}	Bottom
F	Visible	Clearly Visible	<111>	{110}	Bottom
G	Invisible	Visible	<111>	{110}	Bottom
H.	Visible	Visible	<111>	{110}	Middle

Foil Orientation: Between [111] and [012] - 14° from [111]

the theoretical number of displacements/cm^3 under the present irradiation conditions is shown in Table 5.

Table 5

Irradiation Condition	Number of Defects per cm^3	Average Defect Diameter (Å)	Theoretical Number of Displacements/cm^3
As-irradiated	5.04×10^{16}	100	2.92×10^{21}
Irradiated-annealed at 760° (1 hour)	1.44×10^{16}	200	

E. Analysis by Field Ion Microscopy

Micrographs of pure molybdenum tips, prepared from wire specimens, taken at liquid nitrogen temperature, show adequate resolution (Fig. 5). The individual atoms on the (111) planes are not fully resolvable as the field applied to cause field evaporation results in stressing the (111) area. The (011) and (112) planes are clearly resolved.

Micrographs of irradiated molybdenum tips prepared from bulk specimens give slightly distorted images which may be due to poor electropolishing (resulting in asymmetrical tip formation). In one particular sequence, streaking was observed, as shown by the single streak along the (110) planes in Fig. 6. On field evaporation, the streak disappeared leaving behind an incomplete inner ring of (110) atoms. On further field evaporation, complete (110) rings were obtained (Fig. 6). Streak contrast from field-ion micrographs has been discussed elsewhere.[25-27] Considerable streaking has been observed in cold-worked neutron irradiated tungsten[25] and is associated with the interaction of point and line defects. The

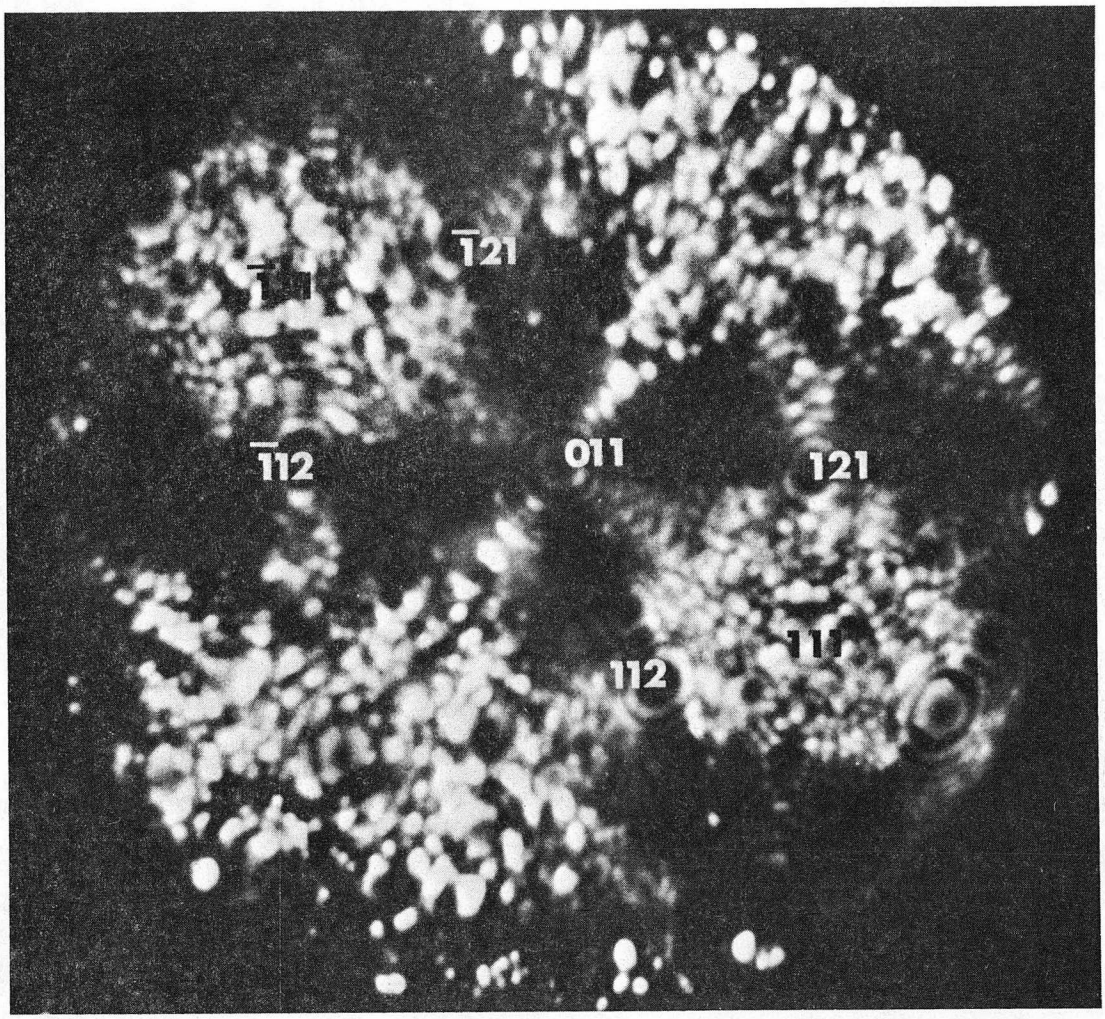

ZN-5924

Fig. 5. Helium field ion micrograph of pure molybdenum at 77°K.

precise role of electropolishing and clustering of interstitial impurities in streak contrast is not known.[25-27]

Other observations on irradiated molybdenum field-ion micrographs included the appearance of bright spots (Fig. 6). The size of these bright spots (a few atom diameters) as well as their enhanced local intensity indicate a local disturbance of the normal arrangement of the material. These may be due to either interstitial atoms bulging out of the surface or due to impurities in the material (see Table 1).

Inspection of some 100 field evaporated {110} planes failed to reveal vacancies. The density of vacancies must be very low, although the reasons for this are not yet known.

IV. DISCUSSION

A. Extension of the Strain Contrast Theory to Radiation Induced Defects in BCC Metals

An interesting observation that can be made from Figs. 2, 3 and 4 is that every one of the analysed strain contrast images have the black side of the black-white image in the direction of the operating diffraction vector in dark field (it can be seen that about 70% of all clearly visible defects have been analysed). On the basis of theory,[14] this would mean that most of the strain contrast images are from interstitial loops. Bell et. al.[13] have pointed out, however, that in FCC systems (primarily aluminum and its alloys) it does not seem possible to unambiguously determine vacancy and interstitial strain fields using strain contrast imaging except for the special case of edge-on defects lying within $t_o/2$ of any surface. The various parameters that have to be considered for both bright and dark field cases have been listed.[13] Figures 7a and 7b show cases where reversals

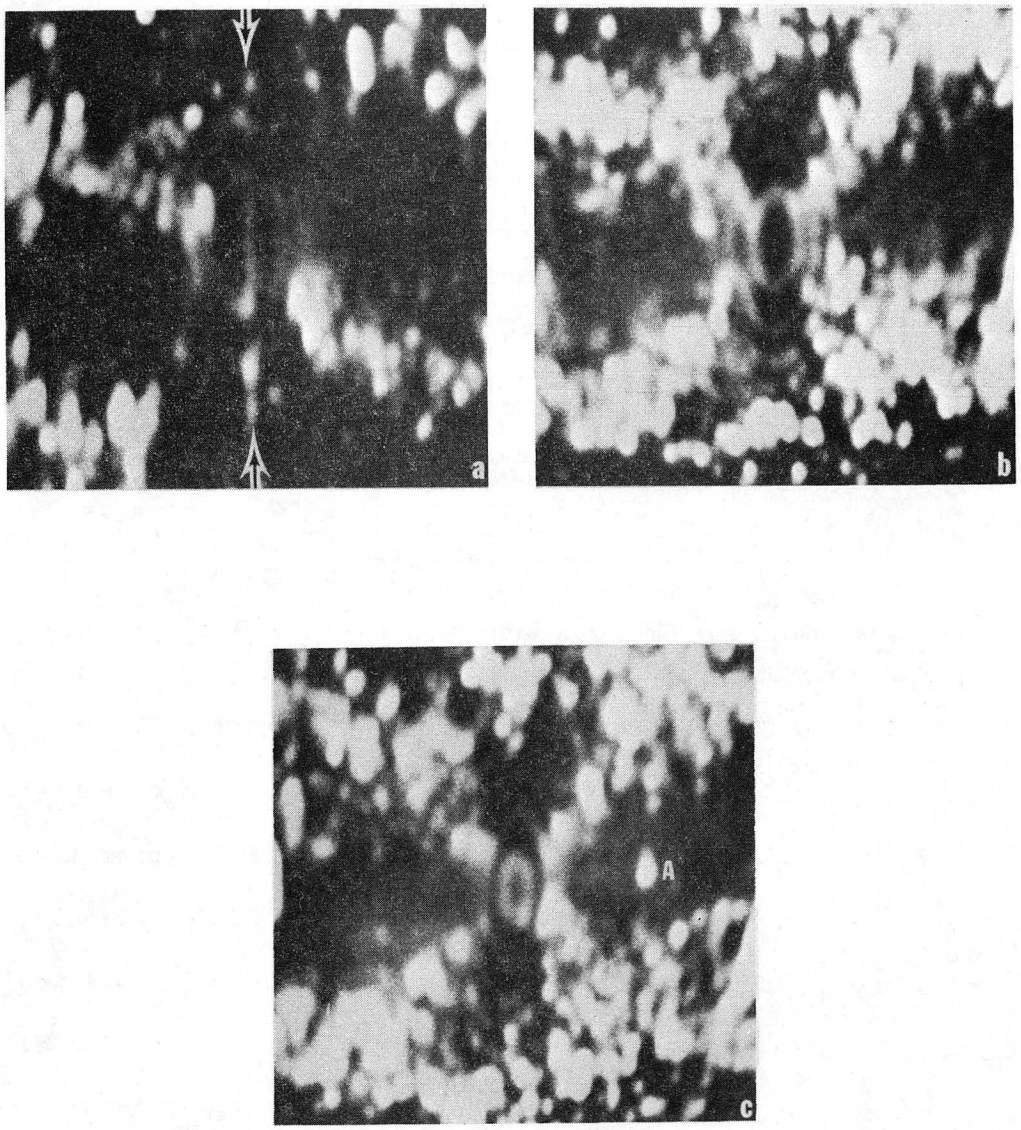

ZN-5933

Fig. 6. Helium field-ion micrographs of irradiated molybdenum tips prepared from bulk specimens. (a) A single streak appears along a ⟨110⟩ plane, and disappears on field evaporation (b); bright spots (A) of a few atom diameters appear in some of the micrographs indicating a local disturbance of the normal arrangement of atoms (c).

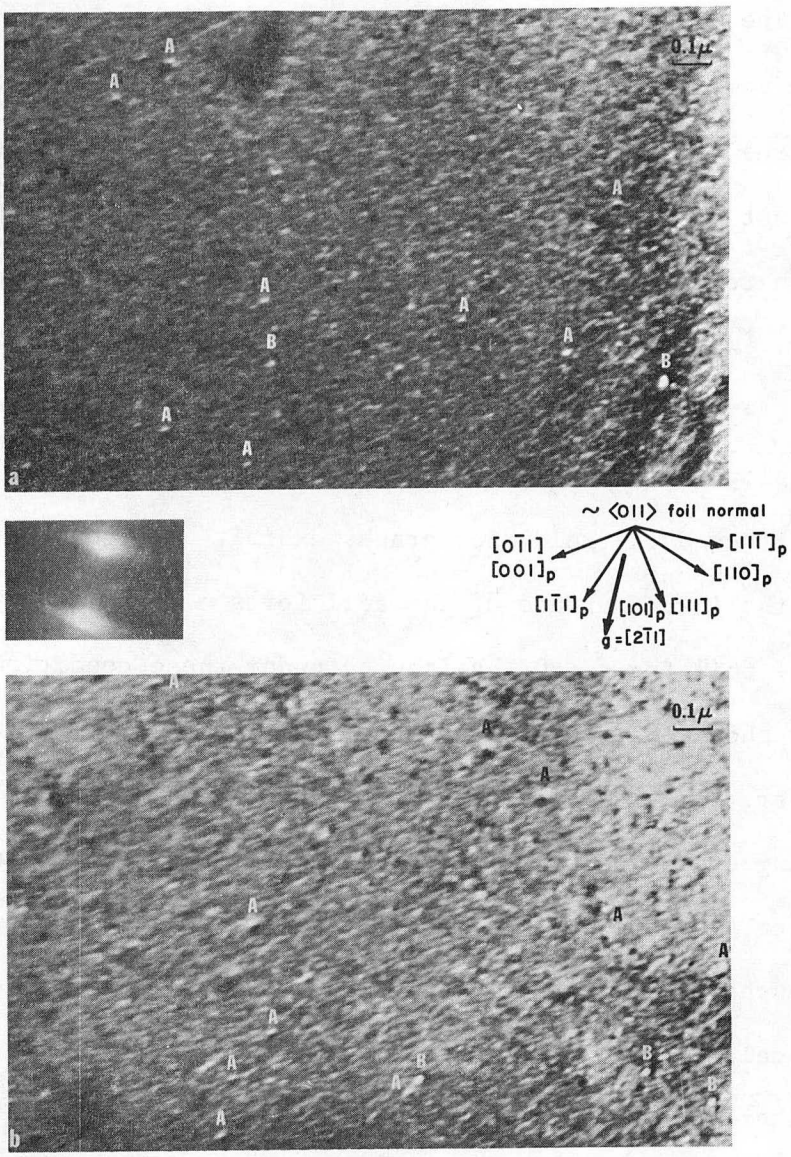

ZN-5923

Fig. 7. Dark field micrographs showing image reversals in irradiated-annealed molybdenum foils at $s < 0$. Defects marked A in (a) and (b) show "interstitial" contrast while defects marked B show "vacancy" contrast. Comparison with the important projected directions alongside show that all the defects marked A are of the type (110) ⟨111⟩ .

of images were observed in irradiated-annealed molybdenum foils at $s < 0$. Even in these cases, the number of "vacancy" type images seems to be few in number.

The streak length of the black and white lobes of the strain contrast image vary with the particular sign of s and position in the foil, although the true diameter (measured along the line dividing the lobes) of the loop does not vary appreciably. In dark field, the white part is equal in length to the dark part (measured along the direction of streaking) at $s = 0$. When $s < 0$, the white part is longer than the black part, while when $s > 0$, the opposite is true because of the change in background intensity that occurs with changing magnitude of s.

Since dark field micrographs exhibit best contrast around defects near the lower surface of the foil for $s > 0$ and near the upper surface of the foil for $s < 0$, by imaging under these conditions (Figs. 3 and 4), it is shown that the induced defects are evenly distributed in the foil. However, defects near the center of the foil will show up under both imaging conditions, especially when the foil is thin and the loops are edge on. However, with higher order reflections, the larger extinction distances are more sensitive to changes in s, making imaging conditions critical. The size of the defect in relation to t_o and the foil thickness is, therefore, of considerable importance, especially in the case of planar defects.

If the specimen is oriented such that the Burgers vector and the normal to the habit plane are both nearly in the plane of the foil, then definite statements concerning the nature of the defects can be made.[13] Table 6 shows the angles between the foil normal and the direction of the Burgers vector, and the normal to the loop plane calculated for three cases.

It can be seen that since the Burgers vector and the normal to the loop plane nearly always lie in the plane of the foil, the conclusions as to defect character should be correct.

Defect density is another factor which can affect the character of strain contrast images. No attempt was made at analyzing the defect structure in as-irradiated molybdenum because of the proximity of other defects.

It has been shown theoretically that the image to be expected from a small defect depends critically upon its position or distance from the foil surface as measured in extinction distances of the operating reflection.[21] This image can either be white on the side of the operating reflection (in dark field) or black on the side of the operating

Table 6

Foil Orientation	<112>	<123>	<123>
Direction of Burgers Vector	$\bar{1}1\bar{1}$	$11\bar{1}$	$11\bar{1}$
Direction of Loop Plane Normal	$\bar{1}10$	$01\bar{1}$	$0\bar{1}\bar{1}$
Angle Between Foil Normal and Burgers Vector	62°	90°	90°
Angle Between Foil Normal and Loop Plane Normal	90°	79.2°	71°

reflection if the defect is half an extinction distance above or below these positions. Using reflections with a longer extinction distance is the recommended solution for causing defects, which may give complications in characterization, to form an image from which the nature of the defect can be unambiguously determined.

For this purpose, the same area of an irradiated-annealed foil of molybdenum was examined using the <112>, <310> and <222> operating reflections in dark field at $s < 0$ such that only those defects near the top of the foil were in good contrast in each case. At $s > 0$, there were very few reversals in image sense.

An increase in the number of strain contrast images was registered with increasing orders of reflection. This would be expected from an increase in the extinction distance, for nearly constant s. A count was made of the number of observable images (> 100Å) with increasing <112>, <310> and <222> reflections (Fig. 8a, b, c), and of the number of "interstitial" and "vacancy" images. The results are summarized in Table 7. It is observed that the number of "vacancy" images decreases with increasing diffraction vector. Similar counts in ion irradiated copper show a decrease in the number of "interstitial" images with increasing diffraction vector.[11] There is a marked decrease in the number of so-called vacancy defects when the <222> reflection is used, but the resolution in dark-field decreases rapidly as the order of reflection increases making the count of the number of "wrong sense" images very approximate. It is observed that the intensity and extent of contrast of the images are reduced with increasing diffraction vector. Since the size of the observed strain contrast images depends on the extent of contrast, the image size decreases with increasing diffraction vector. However, the "wrong-sense" images, which are larger in width for lower order reflections, tend to be of the same size as the "right-sense" images for higher order reflections.

Though, in general, strain contrast imaging techniques do not seem

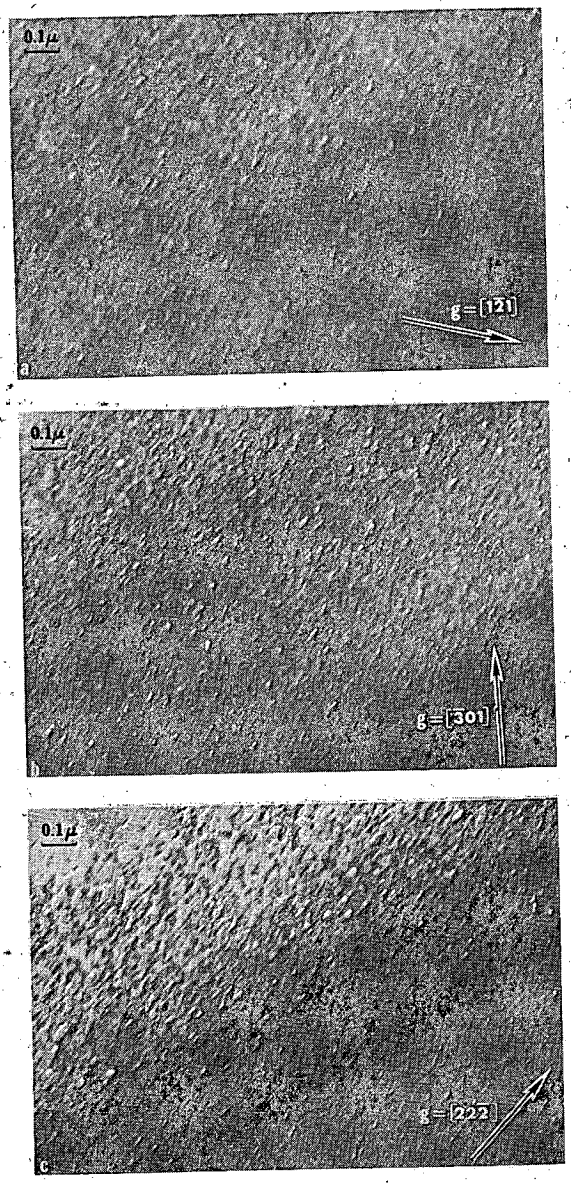

ZN-5932

Fig. 8. Dark field images of the same area at $s < 0$ imaged using different diffraction vectors. The increase in the number of observable images with increasing diffraction vector is evident in (a), (b) and (c) (see Table 5).

to be applicable to the problem of distinguishing between vacancy and interstitial type defects, in this particular case, the evidence presented indicates that the induced defects in neutron irradiated molybdenum are predominantly interstitial in character. It must be noted, however, that the number of parameters that can affect the characterization of these defects are so many[13] that the above conclusions cannot be taken as positive proof of identification.

Table 7

Operating Reflection (hkℓ)	112	310	222
Extinction Distance (Å)	342	472.5	529
Number of Strain Contrast Images	147	286	338
Number of Interstitial Images*	111	239	303
Number of Vacancy Images*	36	47	35
Ratio of Interstitial: Vacancy	12:3	10:2	10:1

* As predicted by strain contrast theory.

B. Irradiation Behavior of Molybdenum

Theory predicts that as primary knock-ons are slowed down, they displace practically every atom that they encounter, creating highly localized regions of damage known as displacement spikes.[28] Regions of dispersed single defects would also be expected in the early stages of the collision sequence since the displacements are widely separated. The spike region itself consists of a central core of vacancies surrounded by interstitial atoms. This arrangement is inherently unstable and will be even more so at elevated temperatures. Interstitial-vacancy recombination

has been shown to occur at temperatures as low as 20°K as a result of electrical resistivity studies on electron irradiated molybdenum.[29] Irradiation at reactor ambient temperature would, therefore, cause considerable self-annealing within the spikes resulting in vacancy-interstitial annihilation. A certain proportion of the interstitials are conveyed away from the spike region by diffusion or by focusing, leaving behind a cluster of vacances. Such vacancy clusters would survive self-annealing, and have been directly observed in a field-ion microscope study of neutron irradiated tungsten.[25] Vacancies in molybdenum have been found to be immobile to 150-200°C.[30] Surviving vacancies can, therefore, be expected to remain as dispersed clusters, while single vacancies from earlier collision sequences will be randomly distributed.

Previous workers on neutron damage in molybdenum have advanced several reasons for the lack of observed vacancies in irradiated molybdenum.[1,2,3] Meakin and Greenfield[2] have shown that impurity-vacancy interactions are probably responsible for the trapping of vacancies. The mobility of the particular defect created by the primary event would decide the future course. Relatively immobile vacancy clusters would grow on annealing to form large defect clusters. Examples marked B in Fig. 7 show perfect vacancy strain contrast in dark field and are larger (size measured along the line of no contrast) than those which show interstitial strain contrast. Interstitials moving away from the spike region are relatively mobile and can contribute to the growth of dislocation loops.

The impurity content has an important role to play in determining

the annealing behavior of irradiated molybdenum. The most likely traps are interstitial impurity atoms. The total interstitial impurity content of molybdenum (carbon and nitrogen) is 1.03×10^{19} atoms/cm^3 (from Table 2). Interstitials created by radiation damage would be attracted by interstitial impurity atoms finally resulting in the development of clusters as more and more interstitials migrate to the trapping centers. Downey and Eyre[1] concluded that the interstitial cluster sizes will depend on the density and distribution of impurity traps.

Annealing characteristics, as indicated by recovery in electrical resistivity and lattice parameter, show a major recovery peak at 150-200°C.[30] This has been attributed to the diffusion of vacancies to interstitial impurities.[30] Since this process does not account for the recovery in lattice parameter, an alternative suggestion[1] is the mutual annihilation of single vacancies and interstitials, following second order kinetics.[31] The recovery of microhardness in the 150-200°C region is also associated with the migration of vacancies to form compact clusters.[1]

Comparing the damage structure of as-irradiated molybdenum with that in irradiated molybdenum annealed at 760°C for 1 hour, the annealing seems to have had little effect on the number of observable defects (Table 3). These results agree with those of Downey and Eyre[1] who attributed the relatively unchanged 500-800°C annealing stage to the break-up of vacancy clusters and the subsequent recombination and mutual annihilation with interstitial clusters in high purity molybdenum.

It is interesting to note that no vacancies were detectable after field ion microscopy of irradiated molybdenum, though bright spots were

observed, which could indicate predominantly interstitial damage. It is not possible at this stage, however, to distinguish between interstitial defects created by radiation damage and interstitial impurity atoms. The high density of interstitial impurity atoms (1.03×10^{19}) prevents definite characterization.

Two types of loops have been observed in BCC metals, with Burgers vectors $\frac{a}{2}$<111> and a<100>. Our observations on the irradiated molybdenum annealed at 760°C for 1 hour indicate that predominantly $\frac{a}{2}$<111> loops are present. Interstitial loops in BCC metals can nucleate on the {110} plane with Burgers vector $\bar{b} = \frac{a}{2}$<110>, enclosing a stacking fault. They can shear in the early stage of growth, in either a <100> or a <110> direction to remove the stacking fault and produce loops with $\bar{b} = \frac{a}{2}$<111> or $\bar{b}$ = a<100>, respectively.[5] This suggests that a <110> shear occurs even at higher temperatures resulting in a large proportion of loops with $\bar{b} = \frac{a}{2}$<111>. Since on annealing to 760°C, there is a predominance of $\frac{a}{2}$<111> loops, it can be assumed that the higher energy <110> shear requires thermal energy to assist it, and would, therefore, occur only at elevated temperatures, as suggested by Eyre and Bullough.[5] All the loops observed by double arc contrast are circular in shape, in keeping with the observation that $\frac{a}{2}$<111> type loops have been predicted to be circular while a<100> type loops retain square shapes.[5] In the 500-800°C annealing stage $\frac{a}{2}$<111> loops predominate, while on annealing to above 1000°C, the higher thermal energy supplied would give rise to a<100> loops, exclusively.

Loops observed by double-arc contrast obey the basic rules set by Bell and Thomas[7] for the identification of prismatic loops in BCC systems.

The loop plane can be uniquely identified for {110} loops though each loop has two possible Burgers vectors of the type $\frac{a}{2}$<111>. These loops are characterized by a major axis along [110] and a minor axis along [001] which is normal to the major axis.

Characterization of the loop plane and Burgers vector of strain contrast images of prismatic loops in irradiated molybdenum follow the image characteristics predicted elsewhere,[7] in that the line of no contrast of{110} <111> loops is normal to the projected <111> direction, and the image is skewed about the line of no contrast in <110>.

V. CONCLUSIONS

Investigation of neutron irradiated molybdenum foils using transmission electron microscopy reveals "black spot" defects in bright field micrographs. It is not possible to determine the nature of these defects by diffraction contrast. Strain contrast imaging provides a means of detecting induced defects which are too small to give rise to any significant diffraction contrast. Bright field micrographs do, however, show characteristic damage structure, such as denuded regions near grain boundaries.

Strain contrast imaging of small defects allows the loop plane and Burgers vector to be analysed, and, to a certain extent, the characterization of the nature of induced damage. Such an analysis is possible by varying the imaging conditions in dark field. Using different operating diffraction vectors in dark field, it has been shown that the lines of no contrast and the direction of streaking of the black-white lobed images are independent of the operating diffraction vector. This shows that the

defects giving rise to strain contrast images are definitely perfect prismatic loops, lying on {110} with $\frac{a}{2}$<111> Burgers vectors. From the relation of the dark field image to the direction of the operating reflection, it is tentatively concluded that the defects are primarily interstitial in character.

Field ion microscopy reveals streaking and image distortion which could arise from several factors, including radiation damage. Interstitial atoms appear as bright spots, but may be confused with impurities present, which give rise to similar contrast. The definite lack of observed vacancies in field ion micrographs can be coupled with previous observations that the damage substructure in neutron irradiated molybdenum is primarily interstitial in nature.

The evidence presented suggest that the defect structure in netron irradiated molybdenum annealed at 760°C for 1 hour consists primarily of interstitial loops with a few comparatively large vacancy clusters. The size of these defects varies from about 100Å in the as-irradiated state to about 200Å in the specimens annealed at 760°C.

ACKNOWLEDGEMENTS

This research was conducted as part of the activities of the Inorganic Materials Research Division of Lawrence Radiation Laboratory, University of California, Berkeley and was done under the auspices of the U.S. Atomic Energy Commission. We are particularly grateful to Dr. J. Moteff of the Nuclear Materials and Propulsion Operation, General Electric Company, Cincinnati, Ohio for supplying the molybdenum and supervising the irradiation.

REFERENCES

1. M. E. Downey and B. L. Eyre, Phil. Mag., 11, 53 (1965).

2. J. D. Meakin and I. G. Greenfield, Phil. Mag., 11, 277 (1965).

3. B. Mastel and J. L. Brimhall, Acta Met., 13, 1109 (1965).

4. B. L. Eyre and M. E. Downey, Sixth International Congress for Electron Microscopy, Kyoto, 1966 (Maruzen Co. Ltd., Tokyo) 385.

5. B. L. Eyre and R. Bullough, Phil. Mag., 11, 31 (1965).

6. M. J. Attardo and J. M. Galligan, Phys. Rev. Letters, 14, 641 (1965).

7. G. Thomas and W. L. Bell, Proc. Honolulu Conference on Lattice Defects, 1965 Gordon & Breach (in press).

8. W. L. Bell and G. Thomas, Phil. Mag., 13, 395 (1966).

9. W. L. Bell, D. M. Maher and G. Thomas, Lattice Defects in Quenched Metals (Academic Press, New York, 1965) p. 739.

10. R. V. Hesketh and G. K. Rickards, Proc. Roy. Soc. A289, 353 (1966).

11. R. V. Hesketh and G. K. Rickards, Phil. Mag., 13, 1069 (1966).

12. W. L. Bell (M.S. Thesis) University of California, Berkeley, UCRL-16024, June, 1965.

13. W. L. Bell, D. M. Maher and G. Thomas, Proc. Harwell Conference, 1966 (in press) UCRL-16955.

14. M. F. Ashby and L. M. Brown, Phil. Mag., 8, 1063 (1963).

15. E. W. Müller, Proc. Fourth International Symposium on Reactivity of Solids, Amsterdam (1960), p. 682.

16. D. G. Brandon, M. J. Southon and M. Wald, Proceedings International Conference on Properties of Reactor Materials and the Effects of Radiation Damage (Butterworths, London, 1961) p. 113

17. M. K. Sinha and E. W. Müller, J. Appl. Phys., 35, 1256 (1964).

18. L. M. Bowkett, L. T. Chadderton, H. Norden and B. Ralph, Phil. Mag., 11, 651 (1965).

19. E. W. Müller, J. Phys. Soc. Japan, 18, Suppl. II (1963).

20. E. W. Müller, Advances in Electronics and Electron Physics, VIII (Academic Press, New York, 1960) p. 83.

21. M. Rühle, M. Wilkens and U. Essmann, Phys. Stat. Sol., 11, No. 2, 819 (1965).

22. P. R. Okamoto, E. R. Levine and G. Thomas, J. Appl. Phys. (in press) UCRL-16897.

23. W. L. Bell and G. Thomas, Phys. Stat. Sol.,

24. G. H. Kinchin and R. S. Pease, Rep. Progr. Phys., 18, 1 (1955).

25. S. Ranganathan, K. M. Bowkett, J. Hren and B. Ralph, Phil. Mag., 12, 841 (1965).

26. D. G. Brandon, Phil. Mag., 13, 1085 (1966).

27. B. Ralph and K. M. Bowkett, Phil. Mag., 13, 1283 (1966).

28. J. Brinkman, J. Appl. Phys., 25, 961 (1954).

29. P. G. Lucasson and R. M. Walker, Phys. Rev., 127, 485 (1962).

30. D. E. Peacock and A. A. Johnson, Phil. Mag., 8, 563 (1963).

31. J. Nihoul, IAEA Symposium on Radiation Damage in Solids, Vol. I, 309 (1962).

This report was prepared as an account of Government sponsored work. Neither the United States, nor the Commission, nor any person acting on behalf of the Commission:

A. Makes any warranty or representation, expressed or implied, with respect to the accuracy, completeness, or usefulness of the information contained in this report, or that the use of any information, apparatus, method, or process disclosed in this report may not infringe privately owned rights; or

B. Assumes any liabilities with respect to the use of, or for damages resulting from the use of any information, apparatus, method, or process disclosed in this report.

As used in the above, "person acting on behalf of the Commission" includes any employee or contractor of the Commission, or employee of such contractor, to the extent that such employee or contractor of the Commission, or employee of such contractor prepares, disseminates, or provides access to, any information pursuant to his employment or contract with the Commission, or his employment with such contractor.